TRIBOLOGIA - Finnish Journal of Tribology 3-4 vol 42/2025

https://doi.org/10.30678/fjt.160136

SUOMEN TRIBOLOGIAYHDISTYS RY
THE FINNISH SOCIETY FOR TRIBOLOGY
www.tribologysociety.fi
https://journal.fi/tribologia

A modified subloading-friction model regularizing the stick-slip transition

Ali Ouzeriat[1], Mohand Ould Ouali[1*], Lahouari Benabou[2]

[1]LEC2M, Mouloud MAMMERI University of Tizi Ouzou, BP 17RP, 15000, Algeria (ouzeriatali@gmail.com)

[2]LISV, Université de Versailles Saint-Quentin-en-Yvelines, France. lahouari.benabou@uvsq.fr

*Corresponding author: mohand.ouldouali@ummto.dz

ABSTRACT

This paper is dedicated to the modeling of friction between solids with a regularized friction model. The proposed model is capable of overcoming the well-known disadvantages of Coulomb-type friction laws. The subloading-friction model, formulated based on the Mroz multi-surface type plasticity theory, is extended to introduce a smooth transition from stick to sliding contact and vice versa during the loading and unloading stages. The formulation includes a slip-memory mechanism and history-dependent effects, with frictional hysteresis, enabling accurate representation of micro-slip accumulation and cyclic energy dissipation. This extension also ensures a smooth and continuous transition between the sticking and slipping contact zones by introducing an adjustable regularization parameter, facilitating efficient implementation in a finite element code. The extended model was successfully implemented into the finite element code Abaqus/Standard using the Fric user subroutine. The extended model was successfully validated by comparison with the analytical solution proposed by Jarzeboski-Mroz for a 2D rectangular block pressed against a rigid substrate, and with the Mindlin-Deresiewicz solution for the problem of a 3D sphere in contact with a rigid plane. Furthermore, comparing the results obtained with Coulomb's law and those described by the extended model shows the significant improvement of the latter in managing the stick-slip transition and reproducing frictional hysteresis.

Keywords: Slip rules, Subloading-friction model, Multi-surface slip, Stick-slip, Numerical Implementation, Abaqus.

1. Introduction

The phenomenon of friction appears at the interfaces between solids in contact. Friction often has a major influence on many applications in engineering design. Frictional contact is an important issue in several areas, like tectonic earthquakes, aerospace, biomechanical systems, forming and metal-cutting processes, and many other industries. In function of its utilization, friction can generate desirable or undesirable effects. Modeling the friction is important because many complex behaviors arise on the interface where friction is the main mechanism governing the material's deformation and degradation (wear, damage ...). However, some difficulties still conditioned the modeling of friction, namely to the poor understanding of this nonlinear phenomenon. Much research has been carried out on finite element computation to describe friction phenomena; see, for instance, [1-4]. The strong nonlinearities of contact interaction due to the unknown contact surface, inequality constraint, and discontinuities in friction relations need treatments with efficient algorithms and an accurate numerical approach to control separately normal and tangential contact stresses. Many studies used the friction Coulomb model, formulated in the framework of the classical plasticity theory, due to its relative simplicity of numerical implementation. Indeed, the Coulomb law presents the inconveniences related to the absence of a one-to-one relationship between the friction forces and the sliding speed, the non-differential character, and the sudden change in the transition from contact with adherence to contact with slipping. To remedy these shortcomings, several works have been carried out. Michalowski and Mroz applied the concept of plasticity to describe the sliding rules of rigid or elastic-plastic bodies with frictional contacts [5]. This is done by considering an analogy between dry contact friction and perfect plasticity. Curnier proposed a relatively general theory of friction compatible with the principles of continuum mechanics [6]. By construction, this theory includes the influence of the normal load on the friction force and can incorporate other mechanisms such as wear, adhesion, [6]. Wriggers et al. discussed the constitutive equations of friction within the framework of elastoplasticity flow rules [7]. Oden and Pires used a non-classical friction law to describe the high nonlinear relation between the friction force and the sliding velocity [8]. Cheng and Kikuchi developed an incremental friction law and used the finite element method to study large deformations in contact problems [9]. Cheikh et al. proposed a phenomenological expression of the friction coefficient depending on an isotropic evolution related to accumulated slip and a kinematic component computed from the actual relative position of the bodies [10]. The new expression of the friction coefficient allows modeling of the friction history without taking into account the evolution of the slip surface. Trzepieciński and Szpunar [11] explored the effect of process parameters on the friction coefficient in single-point incremental forming (SPIF). The study also showed significant differences between the coefficient of friction (COF) at the initial contact and the COF in the stabilized forming zone. While these studies have helped solve important practical problems, extending them to other applications seems risky. Furthermore, focusing solely on the coefficient of friction appears to limit any attempt to generalize or describe other phenomena that may occur, such as wear, cracking, etc. Hence, a need to develop a general model that takes into account the evolution of the sliding surface and can be extended to describe other mechanisms. Hashiguchi et al. [12] analyzed several models and demonstrated the value of the underloading surface model, particularly its detailed description of elastic-plastic and stick-slip transitions for friction and cyclic behavior. However, challenges remain, such as its implementation in commercial software and the associated costs (computation time), which often require the use of pressure-dependent plasticity algorithms and taking into account the change in load surface [13-15]. Also, concerning the contributions related to the numerical implementation of the laws of friction, Oden and Martines established a numerical algorithm for analyzing dynamic frictional phenomena [16]. Giannakopoulos developed a return-mapping algorithm for the integration of friction constitutive relations [17]. In order to achieve the transition from contact with adherence to contact with slipping, friction modeling was extended using the multi-surface plasticity model. This is done after establishing similarities between the behavior at the interface of contact/friction and the classical elastic-plastic theory. By analogy between these two phenomena, Dobry et al. [18] and Jarzebowski and Mroz [19] proposed modeling friction in the framework of the non-classical plasticity theory, based on the concept of multi-surface plasticity. Jarzebowski et Mroz [19] based their work on the solution of elastic spheres in contact under varying oblique forces established by Mindlin and Deresiewics [20]. Sellgren and Olofsson used the analytical solution of elastic spheres to develop a model for a micro-slip range of asperities of constant radius on local and global levels [21]. Hashiguchi et al. incorporated the concept of the sub-loading surface with the smooth elastic-plastic transition to formulate a constitutive equation for friction [22]. Hashiguchi and Ozaki extended the model to take into account the transition from static to kinetic friction, and the viscoplastic behavior due to the creep induced by a high contact pressure over time [23,24].

In this paper, an improved regularized frictional behavior model capable of describing the smooth transition from sticking to sliding is developed. The model is an extension of the subloading-friction model proposed by Hashiguchi et al. [22-24] based on the Mroz multi-surface type plasticity models [15,25-28]. The model is extended to take into account the smooth passage from adhesion contact to sliding contact area and vice versa during the loading and unloading of the friction force. The extension aims to model the evolution of surface adhesion and slip along the contact interface by taking into account the non-linear relationship between the tangential force and the relative speed of sliding of the two bodies in contact, normal pressure, and their distributions. The extended model was implemented via the return-mapping algorithm in the Abaqus/Standard computer code via the Fric subroutine. The numerical results obtained with this model were compared with the 2D and 3D analytical solutions of Jarzeboski-Mroz and Mindlin-Deresiewicz, respectively. The simulation results show that the model correctly describes the analytical results for the two chosen applications.

2. Computation of contact interface problems

Consider two continuous bodies, B1 and B2, that meet each other. For simplicity, let us assume that one of them (B1) is rigid and is moving on the other, deformable body (B2). The motions of the bodies are described by the deformation mapping given by the material point positions. The deformation process occurs when any arbitrary region of the boundary comes into contact. The separation gap gN between two positions is done by:

$$g_N = (\boldsymbol{x}^1 - \boldsymbol{x}^2).\boldsymbol{n} \tag{1}$$

n is the unit outward normal vector on the deformable surface. x1 and x 2 represent position vectors of two material points on (B1) and (B2) respectively. The impenetrability condition can be formulated in the form of the Kuhn-Tucker using the normal contact traction p [29,30]:

$$\mathrm{g_N} \geq 0 \;\; ; \;\; \mathbf{p} \geq 0 \;\; ; \;\; \mathbf{p}.\mathrm{g_N} = 0 \tag{2}$$

The contact problem between two bodies is treated as a boundary condition problem under the assumption of quasi-static small strain. The local equilibrium equation and the compatibility conditions are also considered. The interface behavior between the bodies in contact is characterized by:

- Sticking: no relative tangential movement occurs on the contact interface,
- Sliding: means that a point moves in a tangential direction.

So, the relative displacement $\mathbf{u}$ at the interface may be decomposed into a tangential, $\mathbf{u_t}$, and normal, $\mathbf{u_n}$, components. Tangential displacement consists of reversible and irreversible (slip) parts and can be decomposed in the same way as elastic and plastic behaviors [31]. The same additive decomposition is adopted for the contact traction vector f [32-35]:

$$\mathbf{f} = \boldsymbol{\sigma}.\mathbf{n} = \mathbf{p} + \mathbf{q} = \|\mathbf{p}\|.\,\mathbf{n} + \|\mathbf{q}\|.\,\mathbf{t} \tag{3}$$

with $\mathbf{t} = \frac{\mathbf{q}}{\|\mathbf{q}\|}$, $\mathbf{n} = \frac{\mathbf{p}}{\|\mathbf{p}\|}$

q is the tangential component of f, and t is the tangential unit vectors (Fig. 1). q_1 and q_2 are the components of q in the t_1 and t_2 directions respectively

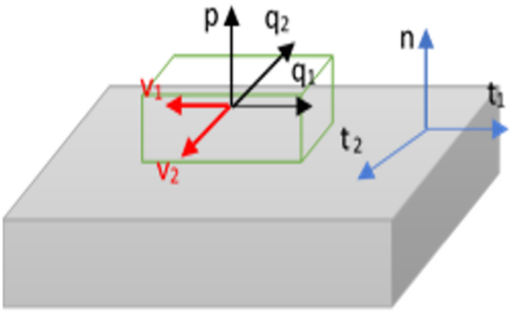

Fig. 1 Local coordinate system for 3-D contact

To resolve the resulting unilateral contact problem (Fig. 2), the penalty method is typically used. The normal traction **p** can be obtained from the multiplication of the penalty factor in the normal direction K_N by the displacement in the normal direction $\mathbf{u_n}$ during contact:

$$\mathbf{p} = K_N \mathbf{u_n} \tag{4}$$

Similarly, the stick (or elastic) component of the tangential traction is:

$$\mathbf{q} = K_T . \mathbf{u_T^e} \tag{5}$$

Where K_T is the penalty factor in the tangential direction.

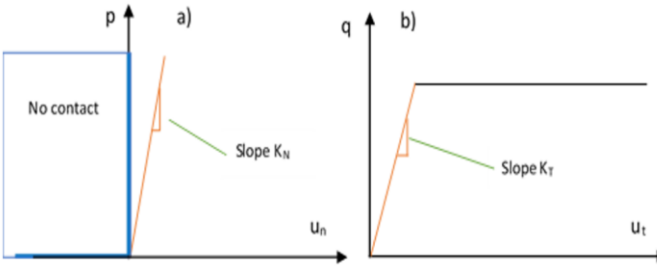

Fig. 2 Schematic of the penalty method: a) normal contact, b) tangential contact

3. Modeling frictional contact

In this section, we present a regularized friction/friction model to overcome the disadvantages of Coulomb-type friction laws, in particular, the sudden transition from contact with adhesion to contact with sliding. This model is an extension of the subloading-friction model that Hashiguichi et al. formulated based on the Mroz multi-surface type plasticity models. We extended this model to smooth the transition of contact from adhesion to sliding and vice versa during tangential force loading and unloading. This extension therefore makes it possible to describe the evolution of surface adhesion and sliding along the contact interface by taking into account the non-linear relationship between the tangential force and the tangential sliding relative to two bodies in contact.

To present this model, we first give some reminders about the contact mechanics. The classical formulation of the Coulomb friction law involves two distinct states: stick and slide, as illustrated in Fig. 3. The law can be written as:

$$\begin{matrix} q < \mu . |p| & \text{and} & \dot{u}_t = 0 \;\; ; \text{sticking} \\ q = \mu . |p| & \text{and} & \dot{u}_t > 0 \;\; ; \text{slipping} \end{matrix} \tag{6}$$

where μ is the friction coefficient.

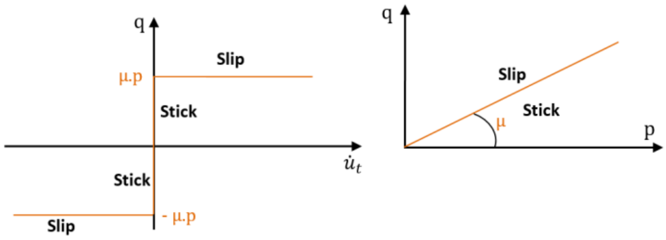

Fig. 3 Representation of the Coulomb friction

The description of the frictional behavior and an incremental stick-slip model derived from the unconventional theory of plasticity of Mroz requires the definition of three features [18]:

1. The friction criterion indicates the force states for which slip occurs.
2. The slip function specifies the modifications of the friction criterion in the course of the slip rule.
3. A slip rule connecting either the slip or the total displacement increment to the force increment.

3.1 Slip friction surface

We adopt the concept of nested friction surfaces inspired by the multi-surface plasticity theory of Mroz [25]. The goal is to describe the evolution of adhesion and partial sliding at the contact interface and to write an incremental relationship in order to model the friction phenomenon from the state of contact stress. The sliding at the contact interface is created during loading by a tangential force, so we can associate the partial sliding with the sliding friction surface Fi. Concerning the total sliding, the friction/sliding surface is associated with the limiting sliding surface FL or the Coulomb friction condition. For each loading step, the partial sliding situation and conditions are represented by the sliding friction surfaces F0, F1,..., Fn, which are similar and concentric cones, moving inside the loading surface. Limit sliding friction FL (Fig. 4). The sliding friction surfaces Fi can be written [18,26,29]:

$$F_i(q_e, \alpha, r) = q_e - R_i = q_e - K_i . \mu p \tag{7}$$

Where Ki is the slip factor, changing between 0 at initial loading to 1 for total sliding, and qe is the equivalent relative tangential traction given by

$$q_e = \sqrt{(q_1 - \alpha_1)^2 + (q_2 - \alpha_2)^2} \tag{8}$$

α_1 , α_2 are located at the center of the slip friction surface in the traction space.

During stick-slip, the contact surface traction lies on the slip friction surface F. This consistency condition can be formulated mathematically as

$$dF = \frac{\partial F}{\partial q_1} dq_1 + \frac{\partial F}{\partial q_2} dq_2 + \frac{\partial F}{\partial \alpha_1} d\alpha_1 + \frac{\partial F}{\partial \alpha_2} d\alpha_2 + \frac{\partial F}{\partial R} dR = 0 \tag{9}$$

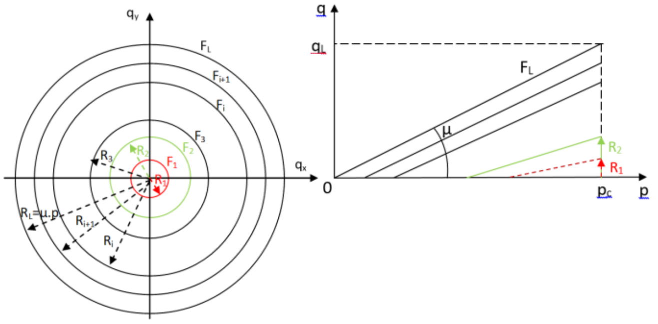

Fig. 4 Configuration of surface friction loading and slip surface limit

Several slip-friction surfaces Fi of size Ri, characterized by slip factor Ki, can be nested within one another due to the different consecutive steps of loading represented in Fig. 5 [18]. Then, as the initiation of a new slip at the traction loading, the translation of the slip surface should respect the isotropic and kinematic movements of the yield surfaces [29] as indicated in Fig. 5. The slip evolution depends on the traction loading represented by moving the slip friction surfaces F_i.

The transition condition from adherence to slipping was generated by active loading of slip surface F_i, moving inside the interior domain bounded by limit slip surface F_L given by the equation:

$$F_L(q_1, q_2, p) = \sqrt{{q_1}^2 + {q_2}^2} - \mu p = 0 \tag{10}$$

The translation of the center of the slip surface between two states of arbitrary loading Fi and Fi+1 has the same normal outward unit ($n_i = n_{i+1}$) [36]. Indeed, the unit normal outward is the same for each active surface Fi and Fi+1 (see Fig.6). It is formulated by

$$n_i = \frac{(q_i - \alpha_i)}{R_i} \quad ; \quad n_{i+1} = \frac{(q_{i+1} - \alpha_{i+1})}{R_{i+1}} \tag{11}$$

So, the final center position is calculated from equation (11) as a function of the initial center:

$$\alpha_{i+1} = q_{i+1} - \frac{R_{i+1}}{R_i}(q_i - \alpha_i) \tag{12}$$

The translation of the slip surface occurs in the same direction as the direction joining the traction point at slip surface R_i with the corresponding point in the next slip surface R_{i+1}. This translation is obtained by the Mroz rule [25,36,37], expressed with vector **m** as:

$$m = (R_{i+1} - R_i)n + \alpha_{i+1} - \alpha_i \tag{13}$$

And the magnitude of translation of the slip surface is determined by [25],

$$d\alpha_i = \varpi(q_{i+1} - q_i) \tag{14}$$

where $\varpi > 0$ is obtained from the consistency condition

The variation of the slip factor Ki (0 ≤ Ki ≤ 1) depends on the slip speed, and it plays the descriptive role of the transition from the passage of total adhesion until reaching total slip with the limit surface FL. The value Ki=1 corresponds to the situation where the contact surface is in total sliding, and the value Ki=0 corresponds to contact with total adhesion. Based on these hypotheses and using

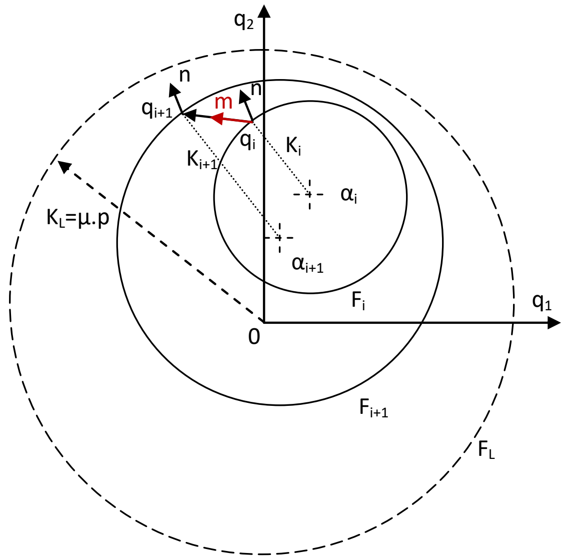

Fig. 5 Kinematics of the proposed model

the ratio size of the subloading surface used by Hashiguchi [22], the evolution of the slip factor can be written as follows [22-35]:

$$\dot{K} = g(K).\|\dot{u}^s\| \quad \text{for} \quad \dot{u}^s \neq 0 \tag{15}$$

The monotone decreasing function g(K) given by Hashiguchi, represented in Fig. 6, could satisfy the condition of the slip factor

$$g(K) = \begin{cases} \to \infty & for\ K_i = 0 \\ 0 & for\ K_i = 1 \end{cases} \tag{16}$$

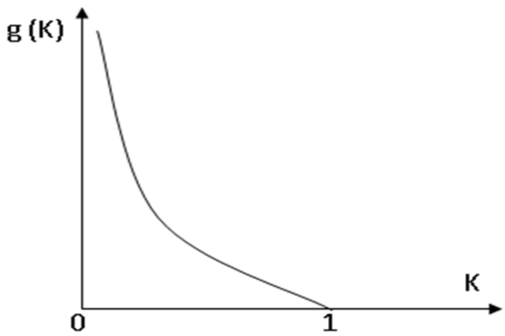

Fig. 6 Function g(K) in the evolution of the slip factor

This function can be formulated by the simple equation [23]:

$$g(K) = -u_b.\cot\left(\frac{\pi}{2}K\right) \tag{17}$$

The slip factor could be formulated by the analytically integrated solution of equation (15) found by Hashiguichi [34], by putting the initial values u_0^s and K0 in the condition of sliding (equal to zero), to describe the isotropic friction/slip surface:

$$K = \frac{\pi}{2}\cos^{-1}\left\{\cos\left(\frac{\pi}{2}K_0\right)\exp\left[-\frac{\pi}{2}u_b\left((u^s - u_0^s)\right)\right]\right\} \tag{18}$$

Where $u^s = \int\|\dot{u}^s\|\,dt$ is the accumulated slip displacement, and K_0 and u_0^s are the initial values of K and u^s, respectively. u_b is a smooth constant.

3.2 Slipping rules of friction

To compute the slip rate, a slip rule is used. The evolution of the slip is assumed to be governed by an isotropic friction law of slip potential defined by:

$$\dot{u}_i^s = \dot{\lambda} n_i \; ; \; i = 1,2 \tag{19}$$

Where $\dot{\lambda}$ is a positive proportionality factor, ni the direction of slip derived from a convex potential G for the non-associated slip rule. $G = \|q - \alpha\|$ governing the initiation of slipping during loading. The center of all slip surfaces is supposed to be at the beginning with equal zero, and only its radius Ri can expand isotropically in stress traction space. To formalize the incremental loading, we used a continuous field for the model instead of a discrete field [38,39]. Under such a hypothesis, $\dot{\lambda}$ is obtained by enforcing the consistency condition dF=0, once we have slipping across the interface.

$$\dot{\lambda} = \frac{\frac{\partial F}{\partial Q}.\mathrm{dQ} - \mu.\mathrm{K}.\frac{\partial F}{\partial p}\mathrm{dp}}{\mathrm{g(k)}.\mu.\mathrm{p}} \tag{20}$$

The evolution relation for the traction increment is obtained from equations (7), (8), and (9) as follows

$$\begin{aligned} \mathrm{dQ} &= K_T(\mathrm{du_t} - \mathrm{du}_t^s) \\ &= K_T\left(\mathrm{du_t} - \frac{\frac{\partial F}{\partial Q}.K_T.\mathrm{du_t} - \mu.\mathrm{K}.\frac{\partial F}{\partial p}\mathrm{dp}}{\mathrm{g(k)}.\mu.\mathrm{p}}.n\right) \end{aligned} \tag{21}$$

Then, the general form of the contact-friction constitutive law is:

$$C_r = \frac{\mu.\mathrm{K}.\frac{\partial F}{\partial p}\mathrm{dp}}{\mathrm{g(k)}.\mu.\mathrm{p}} \tag{22}$$

$$\mathrm{dQ} = \mathrm{K_T^{ep}}.\mathrm{du_t} + C_r.n \tag{23}$$

$$\mathrm{K_T^{ep}} = K_T\left(1 - \frac{1}{\left(K_T + u_b.\mu.p.\cot\left(\frac{\pi}{2}K\right)\right)}\right) \tag{24}$$

Under constant normal pressure (dp=0), the relation between traction increment and tangential displacement increment is reduced to the following equation as follows:

$$\mathrm{dQ} = \mathrm{K_T^{ep}}.\mathrm{du_t} \tag{25}$$

To compute the frictional traction increment for a given displacement increment, we used the continuous slip surface field [38,39] instead of a discrete field, which translates and expands any defined concentric surface with its center initially at the origin. The loading and unloading path for the stick-slip process can be evaluated by imposing the criterion:

$$\begin{aligned} &u^s \neq 0, F = 0 \text{ and } dF = 0 \\ &\quad \text{Loading with slipping} \\ &u^s = 0, F = 0 \; \textit{and } dF < 0 \\ &\quad \text{Unloading without slipping} \end{aligned} \tag{26}$$

Different steps of tangential traction-displacement loading and unloading are presented in Fig. 7.

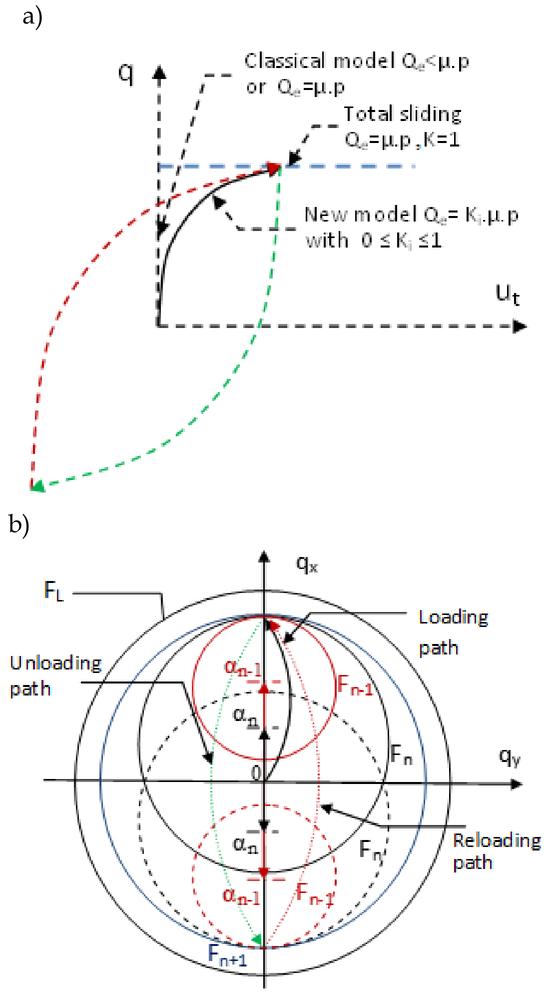

Fig. 7: a) Typical tangential traction-displacement curve; b) slip surface during cyclic loading

3.3 Extension of the Hashiguishi Model

In the present section, we present the extension introduced to the subloading-friction described in the above sections. The extension is introduced to smooth the contact transition from adhesion to sliding and vice versa. To do this, we have modified the slip factor equation proposed by Hashiguishi and co-workers to model the radius of the slip friction surface Ri. Thus, the assumption of stick and slip distinguishes zones depending on the moving slip surface, as shown in Fig. 8, is adopted. Fig. 8 illustrates the stick and slide areas in the two-dimensional (q, p) plane. The active loading is straight lines with slope μ, parallel to the limit line FL (total sliding). For constant normal pressure pc, increasing tangential traction makes the slide apex of a line from zero to adherent pressure pa. The contact area can be divided between the stick area and slide area; each active straight line is associated with slip friction surfaces Fi in the loading space, represented in Fig. 9.

There, the radius Ri (0 ≤ Ri ≤ Ki.μ.p) represents the size of the slipping condition for the active loading slip surface. Jäger [40] found that the size of the stick zone is determined by cones (yield cones) expressed in the force space. So, the tangential stress between two nonrotating half-planes in

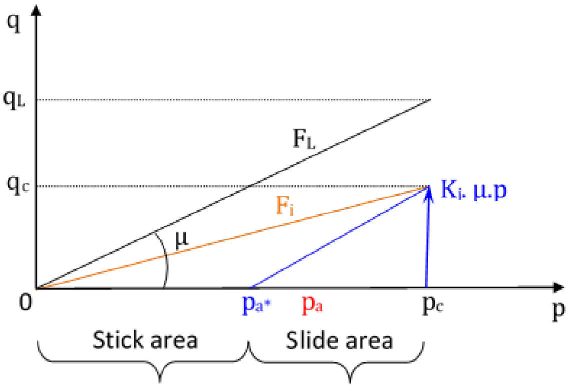

Fig. 8 Stick and slide area with friction line

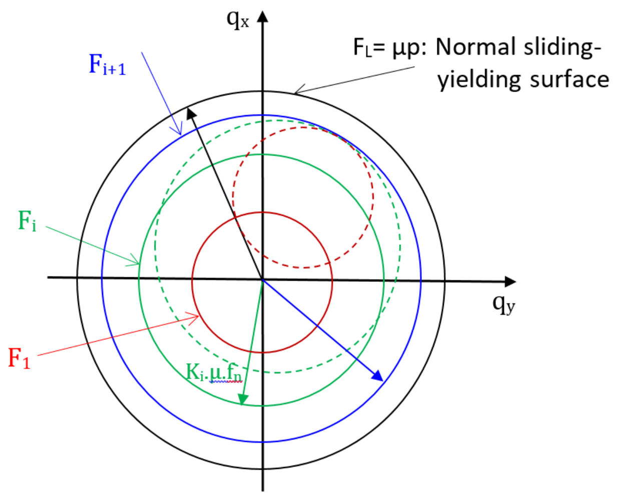

Fig. 9 Stick-slip with active slip friction surface

contact under constant normal and increasing tangential forces is expressed as:

$$q(a, a^*) = \mu(p(a) - p(a^*)) \quad (27)$$

Where a* is the radius of the stick area.

We propose an expression to evaluate the normal pressure contact area and normal pressure in the stick area, as shown in Fig. 8:

$$R_i = \mu p\left(1 - \frac{p_a}{p}\right) = K_i.\mu.p \quad ; \quad p_a = p(1 - K_i) \quad (28)$$

Where pa is the normal pressure applied in the virtual stick contact area, which equals zero at total sliding and equal contact pressure at full stick. Considering equivalent load history for loading, unloading, and reloading, the reverse slip area expands from the loaded enclosed by the slip surface Fi.

4. Numerical implementation

The modified subloading-friction model described in the above section has been implemented into the finite element code Abaqus through a "FRIC" user subroutine [41]. The advantage and novelty of this extension lie in its ability to account for slip memory and hysteresis. From a practical standpoint, we judiciously coupled the slip factor proposed by Hashiguchi to account for the isotropic extension of the slip surface with the kinematic translation phenomenon of this slip surface, as described by Mroz. The implementation procedure is described below. In order to find the updated solution at time step (n+1), we start the calculation by assuming elastic trial contact traction. q_{n+1}^{Tr}, and the slip surface is defined concentric with their center, α is at the origin, equal to zero, if q_{n+1}^{Tr} lies inside the loading slip surface in the previous time step n, it is judged that the calculation as the sticking contact process was correct, q_{n+1}^{Tr} is determined as the correct traction q_{n+1}^{final} in the step (n+1), however, if q_{n+1}^{Tr} lies outside the loading slip surface, previous time step n, it is judged that the calculation as a sticking contact process was incorrect, so a sliding relaxation has been introduced until the loading slip surface is satisfied as follows:

$$\begin{aligned} f(Q_{n+1}^{Tr}) \le R_n\!: \ \dot{u}_{n+1}^{s} = 0, \quad & Q_{n+1}^{final} = Q_{n+1}^{Tr} \\ f(Q_{n+1}^{Tr}) > R_n\!: \ \dot{u}_{n+1}^{s} \neq 0, \quad & Q_{n+1}^{final} \neq Q_{n+1}^{Tr} \end{aligned} \quad (29)$$

Evaluate the frictional behavior with the slip criterion at the time (n+1) as:

Assume all contact areas are stick

1 –Elastic predictor computation (sticking)

$$q_{n+1}^{Tr} = q_n + K_T.\Delta u_{n+1} \quad (30)$$

2- Verification of slip / stick condition

If: $F_{(n+1)} = Q_{e\ (n+1)}^{tr} - K_{(n)}.\mu.p < 0$ sticking state

Else: slipping state occurs.

3- Slip corrector

$$\Delta u_s = \Delta\lambda \frac{\partial F}{\partial q} \quad (31)$$

$$q_{n+1} = q_{n+1}^{tr} - K_t.\Delta\lambda\, n_{n+1} \quad (32)$$

$$F_{(n+1)} = Q_{e_{i(n+1)}} - R_{(n+1)} = 0 \quad (33)$$

Generally, the computed non-linear equation function of slipping Δus for surface loading F(n+1)=0, the update slipping process depends on the parameter Δλ, which is calculated with an iterative procedure after linearization of the consistency condition of F(n+1)=0. Fig. 10 illustrates the geometrical interpretation of the sticking predictor and slipping corrector.

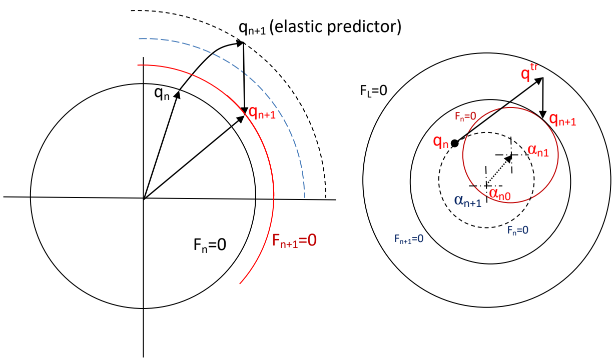

Fig. 10 Schematic of sticking predictor / slipping corrector

Using the additive incremental small displacement decomposition of the sticking and slipping contribution, we obtain the tangential force at the end of the step

$$q_{n+1} = q_n + K_T \Delta u_t - K_T.\Delta u^s$$

$$q_{n+1} = q^{tr}_{n+1} - K_T.\Delta\lambda\, n_{n+1} \qquad (34)$$

Let the unit tangential vector:

$$n^{tr}_{n+1} = \frac{q^{tr}_{n+1} - \alpha^{tr}_{n+1}}{\|q^{tr}_{n+1} - \alpha^{tr}_{n+1}\|} \;\; ; \;\; n_{n+1} = \frac{q_{n+1} - \alpha_{n+1}}{\|q_{n+1} - \alpha_{n+1}\|} \qquad (35)$$

The unit vector at the end of the step has the same direction of traction, so:

$$q_{n+1} - \alpha_{n+1} = n^{tr}_{n+1}\|q_{n+1} - \alpha_{n+1}\| \qquad (36)$$

$$q^{tr}_{n+1} - K_T.\Delta\lambda - \alpha^{tr}_{n+1} = n^{tr}_{n+1}\|q_{n+1} - \alpha_{n+1}\| \qquad (37)$$

Making a substitution into equation (37) leads to

$$\|q_{n+1} - \alpha_{n+1}\| = \|q^{tr}_{n+1} - \alpha^{tr}_{n+1}\| - K_T.\Delta\lambda_{n+1} \qquad (38)$$

during the slipping condition, the slip surface F can be obtained in terms of $\Delta\lambda$ as

$$F = Q_{e(n+1)} - R_{(n+1)} = Q^{tr}_{e\;(n+1)} - K_T.\Delta\lambda_{n+1} - R_{(n+1)} = 0 \qquad (39)$$

This nonlinear equation may be solved using the Newton-Raphson procedure with unknown $\Delta\lambda$.

5. Numerical applications

The modified subloading-friction model has been implemented into the finite element code Abaqus, through a "FRIC" user subroutine, and used to assess its capability to describe two frictional contact examples in 2D and 3D. The choice of these two applications is motivated by the availability of analytical solutions.

5.1. Rectangular block on a rigid foundation

In this section, the extended friction model is applied to a 2-D elastic block pressed against a rigid substrate. This application was studied analytically by Jarzebowski and Mroz [26]. The height and width of the rectangular block are, respectively, 10mm and 2mm. The behavior of the block is assumed elastic with Young's modulus E = 200 GPa and the Poisson's ratio ν = 0.3. After a uniform mesh stability analysis, the block is meshed with 8000 four-node plane stress quadrilateral elements (CPS4R), as shown in Fig. 11. The rigid base is fully constrained. The simulation is carried out in two steps. In the first step, the elastic block is subjected to compression by applying a uniform pressure of p=40 MPa at the upper surface. In the following second step, the normal pressure is kept constant, and a tangential loading is applied at the lateral surface by imposing a displacement ut=0.001mm. The friction coefficient is taken as μ=0.15.

In order to achieve the cyclic loading, an alternating loading between ut = 0.001 mm and ut = -0.001 mm is applied in the lateral surface, while keeping the normal pressure constant.

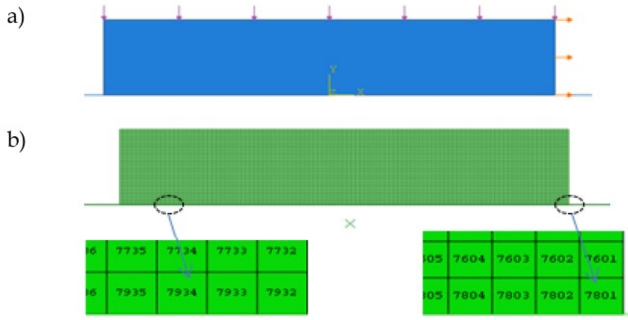

Fig.11 Rectangular block in contact with rigid base: a) boundary conditions; b) mesh and elements (7934 and 7801) in the contact zone used for the post-processing

Fig. 12 shows the distribution of the von Mises stress at the end of each calculation step. Fig. 12a represents the response of the material to the application of only the normal pressure using the modified subloading-friction model (Fric subroutine). We obtain practically the same stress distribution with both models. The von Mises stress distribution is symmetric (without applied tangential loading). Fig. 12b and Fig. 12c represent the distribution of the von Mises stress after applying a combined loading (normal pressure and tangential loading). Fig. 12b is obtained using the Fric subroutine, and Fig. 12c is the classical Coulomb friction law available in Abaqus. As expected, the von Mises stress distribution is symmetric without applying tangential loading. The peak values of the von Mises stress are observed near the bottom surface (in contact) of the elastic block. The application of the tangential loading (horizontal displacement u =0.001mm) creates an asymmetry in the distribution of stresses, using the two models. The maximum stress zone now appears on the lateral face where the tangential loading is applied (namely, the finite element 7801). We can also observe that this loading induces the formation of two contact zones: stick and slip areas.

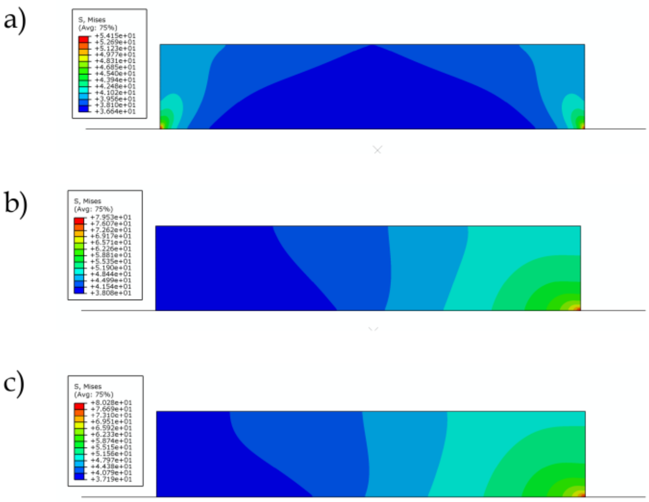

Fig.12 Von Mises stress distribution during a) normal loading (Fric), b) Combined loading (Fric), c) Combined loading (Coulomb law)

Fig. 13 shows a comparison between the curves obtained with the modified subloading-friction model (Fric) and the Coulomb model available in Abaqus with the analytical solution of Jarzebowski and Mroz [26]. The curves represent the evolution of the tangential load versus the relative tangential displacement under a cycle of loading. The one-cycle loading-unloading curve is obtained by imposing a relative tangential displacement varying between -1µm and 1µm.

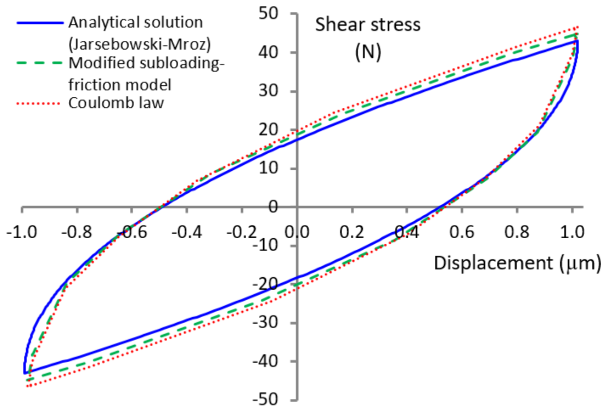

Fig. 13 Hysteresis force-displacement curve for an elastic block on a rigid foundation.

The hysteresis loop is correctly described by both models. However, the curve obtained with the modified subloading-friction model is closer to the analytical solution of Jarzebowski and Mroz than that obtained with the Coulomb model. In order to analyze these results in more detail, we give in Fig. 14 the part of the curve that corresponds to the start of loading (loading stage). It appears from this figure that the numerical results of the modified subloading-friction model are very close to the analytical solution in comparison with the Coulomb model.

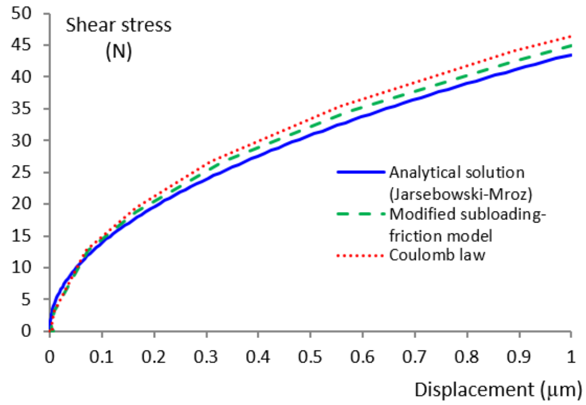

Fig.14 Relationship between the tangential load vs tangential displacement for the elastic block.

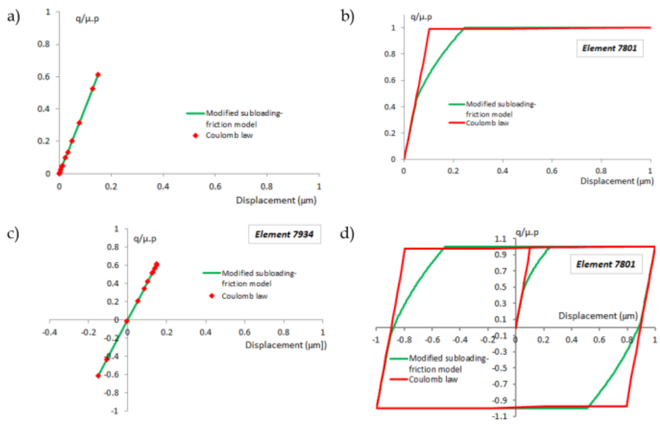

Fig.15 Normalized tangential traction versus relative tangential displacement. a) element 7934; b) element 7801, c) local cyclic contact element N°7934, d) local cyclic contact element N°7801 (Fig. 11b)

Fig. 15 shows a comparison of the evolution of the normalized tangential traction load versus relative tangential displacement. These curves are obtained at the contact elements 7801 and 7934 (Fig. 11b) using the modified subloading-friction model (Fric) and the Coulomb law. Figures 15a and 15b are obtained under monotonic loading. From these results, we can see that the extended subloading-friction model was successfully validated by comparison with the analytical solution proposed by Jarzeboski-Mroz for a 2D rectangular block pressed against a rigid substrate.

Figures 15c and 15d represent the material response to one-cycle loading. The simulations were carried out with a constant pressure distribution on the contact surface. At the local level, a difference in behavior is observed during the transition between adhesion and slip, demonstrating the value of the regularization introduced in our model, as illustrated in Fig. 15. A difference in behavior is observed during the transition between sticking and slipping. While the Coulomb model describes a near-instantaneous, abrupt transition, the regularized subloading-friction model (Fric) describes a gradual, smoothed transition. As we can see in Fig. 15b and 15d, the modified subloading-friction model describes the smooth transition from the stick to the slip zone during both the loading and unloading phases. So, the significant improvement of the results in managing the stick-slip transition is also shown in reproducing frictional hysteresis.

Indeed, Fig. 16 shows a comparison of the profiles of the distribution of the normalized stress versus the relative displacement in the two elements 7801 and 7934. The element 7934, located far from the face where the tangential loading is applied, has reversible contact behavior (stick contact) under both monotonic (15a) and cyclic (15c) loadings. However, as shown in Figures 15b and 15d, the contact element 7801 presents a stick behavior at the start of loading, then a slip behavior. In Fig. 15, the whole point of using the modified subloading-friction model (Fric) appears, which allows a non-brutal (regularized) transition from the stick zone to the slip zone. We also observe that the local hysteresis is qualitatively better described with the modified subloading-friction model.

Fig.16 shows the shear traction evolutions computed with the modified subloading-friction model (Fric) and the Coulomb law for different step time loading. A good agreement was found between the two laws. This agreement is observed before and after the application of tangential displacement.

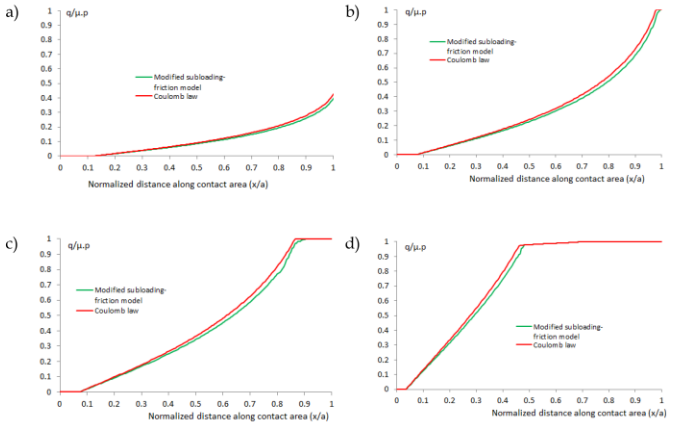

Fig. 16 Shear traction distribution at different times: a) t=1.11, b) t=1.25, c) t=1.39, d) t=1.58, e) t=2

5.2 3D-Elastic sphere on a rigid surface

The second application of the modified subloading-friction model (FRIC) is carried out in 3D. This application is used to study the frictional contact problem with slip and adhesion between elastic bodies, commonly called the Cattaneo–Mindlin problem [44]. The constitutive material of the quarter-sphere with a radius of 10mm is assumed to be elastic with a Young modulus of 200 GPa and Poisson's ratio of 0.3. Due to symmetry considerations, a quarter-sphere is placed in contact with a rigid plate as shown in Fig. 17a. A normal pressure p=2.5MPa is applied on the top surface. While keeping the normal pressure constant, a tangential displacement is applied to create friction conditions. The imposed tangential displacement is ux =0.0089mm (Fig. 20a). The friction coefficient of the contact zone is μ=0.1.

A mesh stability study showed that gradually increasing the element size from the contact region toward the upper surface of the quarter-sphere provides an effective balance between accuracy and computational efficiency. The final mesh consists of 56,309 eight-node linear brick elements with reduced integration (C3D8R), as shown in Fig. 17b. In the contact region, the finest mesh resolution used corresponds to an element size of approximately 5μm.

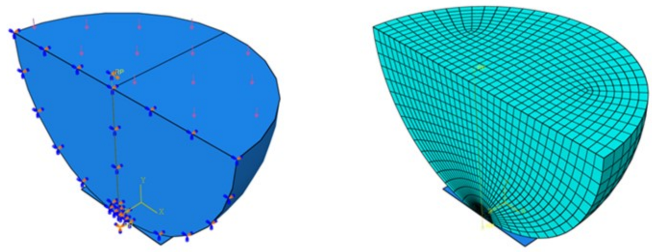

Fig. 17 Half-sphere in contact with rigid flat: a) boundary conditions; b) Mesh

The simulations of this problem are carried out using the modified subloading-friction model implemented into Abaqus using the Fric subroutine. The numerical results of normal-pressure distribution are compared to the analytical solution of Hertz in Fig. 18. Good agreement was also found between the numerical and the analytical Hertz solutions in the case of 3D simulation.

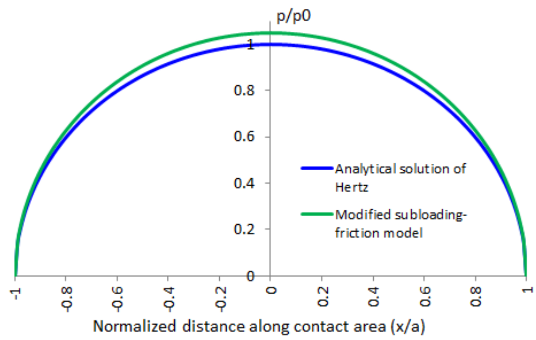

Fig. 18 Pressure distributions

Fig. 19 gives the variation of tangential traction force distribution along the contact interface. The figure represents a comparison between the modified subloading-friction model (Fric) and the Coulomb model available in Abaqus with the analytical solution of Mindlin.

The profile at the contact interface displays adherence and slip areas. The stick portion is located in the frame: -0.5<x/a<0.5. We observe that the modified subloading-friction model reproduces correctly the Mindlin analytical solution as well as the Coulomb law. However, the results of the extended model are more precise.

Fig. 20 shows a comparison of the tangential load ratio, $\frac{Q}{\mu P'}$, obtained numerically and the modified subloading-friction model (Fric) and the Coulomb model analytically under three different loadings: monotonic loading (Fig. 20a), loading-unloading (Fig. 20b), and one cycle loading (Fig. 20c). The curves represent the evolution of the tangential load ratio versus the tangential displacement ratio, at a normal force constant.

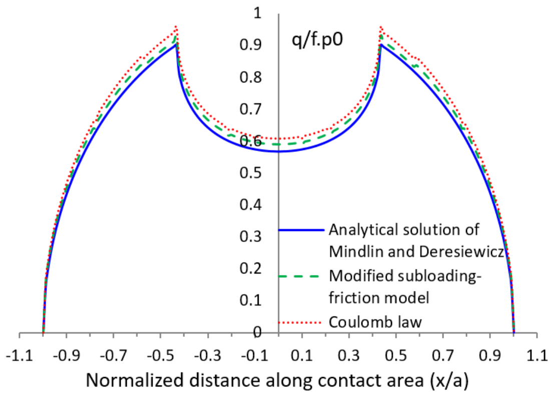

Fig. 19 Tangential traction force distribution

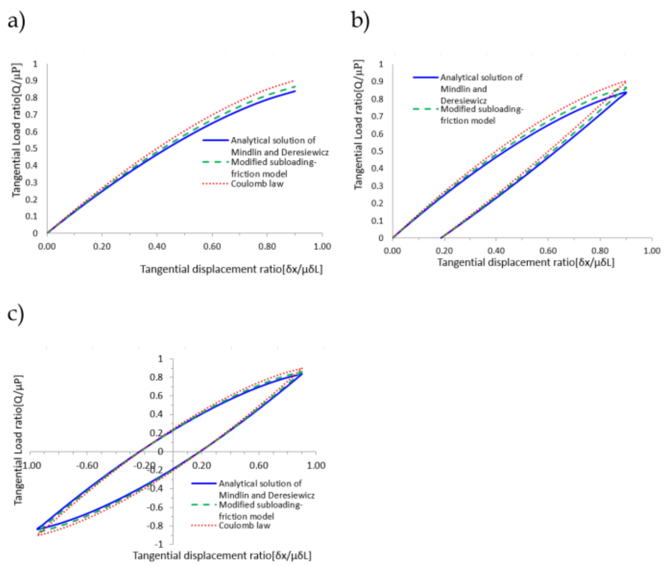

Fig. 20 Comparison of the tangential load ratio obtained numerically and analytically for three loading scenarios: a) monotonic loading; b) loading-unloading; c) one cyclic loading

The three figures show that the modified subloading-friction model describes the analytical solution better than the Coulomb law. Fig. 20b illustrates the energy loss due to the friction for elastic contact caused by slipping at the interface. Indeed, when the tangential force decreases to zero, after reaching the maximum value Qm, a complete adhesion occurs at this point, and the tangential displacement decreases to a non-zero value δr, called residual displacement. This figure also shows the benefit of a regularized transition when moving from the stick to the slip contacts, which appears when approaching the maximum value of the tangential force. Fig. 20c shows hysteretic loop forms during oscillating tangential force

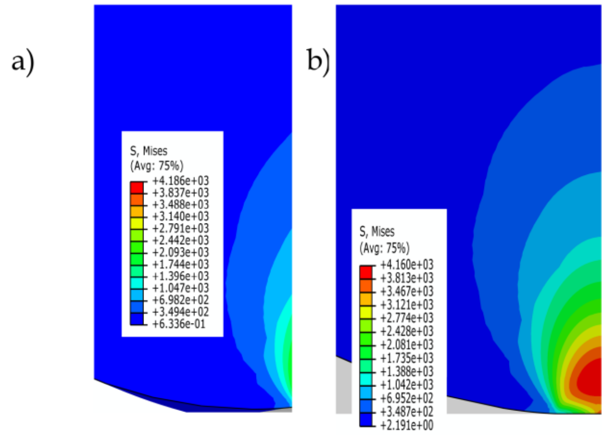

Fig. 21 Von Mises stress during tangential loading predicted with: a) Coulomb law, b) modified subloading-friction model (Fric)

while keeping the normal pressure constant.

The numerical curve obtained using the modified subloading-friction model (Fric subroutine) is in concordance with the analytical solution of Mindlin and Deresiewicz [20]. So, we can also attest in the case of a 3D simulation that the modified subloading-friction model validates the analytical solution proposed by Mindlin-Deresiewicz for the problem of a 3D sphere in contact with a rigid plane. Additionally, the comparison of the results obtained with Coulomb's law and those described by the extended model, made in Figures 20b and 20c, shows the significant improvement in the frictional hysteresis loop. Moreover, the energy dissipations, representing the area of the zone bounded by the force-displacement hysteresis loop, obtained numerically (Fric subroutine) and analytically by Mindlin and Deresiewicz are very close.

Fig. 21 shows the distribution of the von Mises stress obtained with the Coulomb law and the modified subloading-friction model. We observe in Fig. 21 a little difference between the two models for the numerical distribution of the von Mises stress in the deformed sphere.

6. Conclusion

In this work, we proposed a modified subloading-friction model based on the analogy between plasticity and contact-friction theories in solids. The modification concerns the regularization (smoothing) of the transition from stick to slipping. The latter concisely describes the friction phenomena of solids by adopting a stick-slip decomposition similar to elastoplastic decomposition in solids. The continuity of the transition from the sticking zone to a slipping zone at the contact interface is formulated through a smooth relationship between the friction stress and the tangential displacement. It makes it possible to describe the evolution of the active friction load surface. This regularized model offers a significant improvement compared to the classic friction model because it ensures continuity through an incremental equation addressing the lack of a one-to-one relationship between friction forces and slip velocity. It also overcomes the non-differential character of the Coulomb-type friction laws. The extended model allows the incorporation of the slip-memory mechanism and history-dependent effects, including frictional hysteresis. So the micro-slip accumulation and cyclic energy dissipation can now be described. This model was implemented into the finite element code Abaqus using a Fric user subroutine. An incremental iterative solution was established to simulate the nonlinear friction problem. The implementation of the friction constitutive equation was successfully carried out using a return mapping algorithm. The regularized subloading-friction model has been successfully applied to 2D and 3D applications. The numerical results obtained using this model were successfully compared with the analytical solutions of the two problems considered: the solution of Jarzebowski-Mroz [26] for the first application and Mindlin-Deresiewicz [20] for the second application. The comparison with the numerical results obtained with Coulomb's law demonstrates the capacity of the extended model to describe the smooth stick-slip transition in the 2D and 3D cases. It also offers the advantage of reproducing the frictional hysteresis loop.

As a perspective on this work, we plan to apply it in the context of metal forming. Indeed, realistically modeling manufacturing processes requires the accurate reproduction of the mechanical interaction between contacting surfaces. The goal is to accurately describe the forming forces, the power required, and the stresses on the tools under contact conditions that depend on pressure, surface finish, temperature, lubrication, and slip rate. Hence, the value of an advanced friction model. Another important extension that we are currently working on is the consideration of anisotropic friction. In Coulomb-type laws, this is done by considering the friction coefficient becomes a tensor or a function of the sliding direction, often relative to a material axis. In the present model, another approach, namely based on the definition of an anisotropic slip surface, is necessary. So, a fine description of the isotropic and cinematic evolution of this surface in the framework of this assumption is another challenge.

Annex:

The global equations from the discretization of the virtual work principle are available in Abaqus. The global equilibrium equation to be updated from time tn to time tn+1 can be written:

$$\mathrm{F_{ext}} - \mathrm{F_{int}} + \mathrm{F_c} = \mathrm{R_{res}} \tag{A1}$$

$\mathrm{F_{ext}}$, $\mathrm{F_{int}}$ and $\mathrm{F_c}$ are external, internal, and contact forces, respectively. Rres is the residual vector.

Abaqus/Standard uses an iterative implicit calculation (Newton-Raphson method) to solve the nonlinear equilibrium equation (38) for a displacement U_{n+1}^{i}:

$$(K)_{n+1}^{i}\Delta U_{n+1}^{i+1} = -(F_{int})_{n+1}^{i} + (F_{ext})_{n+1} + \left(F_c(U_{n+1}^{i+1})\right)_{n+1}^{i+1} \tag{A2}$$

i refers to the ongoing iteration, and n refers to the loading increment. K is the tangent stiffness matrix:

$$\mathrm{K}_{n+1}^{i} = \frac{\partial \mathrm{R}_{\mathrm{res}(n+1)}^{i}}{\partial \mathrm{U}_{n+1}^{i}} \tag{A3}$$

The implicit solution is conducted incrementally and iteratively. The increment displacement, solution of the problem in Abaqus, is split into two parts: without contact detection $(\Delta U_{lib})_{n+1}^{i+1}$, and a term depending on the contact problem $(\Delta U_c)_{n+1}^{i+1}$.

$$\Delta U_{n+1}^{i+1} = (\Delta U_{lib})_{n+1}^{i+1} + (\Delta U_c)_{n+1}^{i+1} \tag{A4}$$

With

$$(\Delta U_{lib})_{n+1}^{i+1} = \left((K)_{n+1}^{i}\right)^{-1}\left(-(F_{int})_{n+1}^{i} + (F_{ext})_{n+1}\right) \tag{A5}$$

And

$$(\Delta U_c)_{n+1}^{i+1} = \left((K)_{n+1}^{i}\right)^{-1}\left(\left(F_c(U_{n+1}^{i+1})\right)_{n+1}^{i+1}\right) \tag{A6}$$

The determination of the solution of Eq. 43 at each increment (n+1) needs the calculation of the contact force $F_c\left(U_{n+1}^{i+1}\right)$ which depends on the local traction force q(n+1). In this study, $q_{(n+1)}$ is calculated using the regularized friction model presented in the above section. To estimate $q_{(n+1)}$, a return mapping algorithm is carried out by first calculating the elastic predictor (sticking contact) taken as an initial condition, followed by plastic correction (sliding contact), if slip takes place [42,43]. So, the updating scheme consists of the determination of the stress traction q(n+1) corresponding to the (n+1) increment, knowing the stress traction q(n) and the tangential displacement u(n), already calculated in the incremental increment (n).

Acknowledgments

The authors thank Professor Zenon Mroz for his fruitful advice.

Conflicts of interest

The author(s) declared no potential conflicts of interest with respect to the research, authorship, and/or publication of this article.

Funding statement

The author(s) declared that this research received no specific grant from any funding agency.

References

[1] R. Djeridi, M. Ould Ouali, Experimental modeling of wear behavior of filled elastomer SBR under dry friction - Influence of roughness. Key Engineering Materials, vol. 640, 13-20, 2015. http://dx.doi.org/10.4028/www.scientific.net/KEM.640.13

[2] Z. Yang, X. Deng, Z. Li, Numerical modeling of dynamic frictional rolling contact with an explicit finite element method. Tribology International, vol. 129, 214-231, 2019. https://doi.org/10.1016/j.triboint.2018.08.028

[3] G. Franz, K. E. Agode, S. Panier, T. Lesage, Finite element modeling of ASTM-G98 galling test - Numerical study of stress distributions in stainless steel specimens. Jurnal Tribologi, vol. 25, 102-118, 2020.

[4] A.C. Messellek, M. Ould Ouali, A. Amrouche, Adaptive finite element simulation of fretting wear and fatigue in a taper junction of modular hip prosthesis. Journal of the Mechanical Behavior of Biomedical Materials, vol. 111, 103993, 2020. https://doi.org/10.1016/j.jmbbm.2020.103993

[5] R. Michalowski, Z. Mroz, Associated and non-associated sliding rules in contact friction problems. Archives of Mechanics, vol. 30, 259–276, 1978.

[6] A. Curnier, A theory of friction. International Journal of Solids and Structures, vol. 20, no. 7, 637–647, 1984. https://doi.org/10.1016/0020-7683(84)90021-0

[7] P. Wriggers, T.V. Van, E. Stein, Finite element formulation of large deformation impact-contact problems with friction. Computers & Structures, vol. 37, 319–331, 1990. https://doi.org/10.1016/0045-7949(90)90324-U

[8] J.T. Oden, E.B. Pires, Nonlocal and nonlinear friction laws and variational principles for contact problems in elasticity. Journal of applied mechanics, vol. 50, 67-76, 1983. https://doi.org/10.1115/1.3167019

[9] J. Cheng, N. Kikuchi, An incremental constitutive relation of unilateral contact friction for large deformation analysis. Journal of Applied Mechanics, vol. 52, no. 3, 639–648, 1985. https://doi.org/10.1115/1.3169114

[10] M. Cheikh, S. Quilici, G. Cailletaud, Presentation of KI-COF, a phenomenological model of variable friction in fretting contact. Wear, vol. 262, no. 7–8, 914-924, 2007. https://doi.org/10.1016/j.wear.2006.10.001

[11] T. Trzepieciński and M. Szpunar. Prediction Of The Coefficient Of Friction In The Single Point Incremental Forming Of Truncated Cones From A Grade 2 Titanium Sheet. TRIBOLOGIA - Finnish Journal of Tribology, 1-2 vol 40, 2023. https://doi.org/10.30678/fjt.127844

[12] Hashiguchi, K., Yamakawa, Y., Anjiki, T. et al. Comprehensive Review of Subloading Surface Model: Governing Law of Irreversible Mechanical Phenomena of Solids. Arch Computat Methods Eng 31, 1579–1609 (2024). https://doi.org/10.1007/s11831-023-10022-1

[13] Aravas, On the numerical integration of a class of pressure-dependent plasticity models, Int. J. Numer. Methods Engrg. 24 (1987) 1395–1416. https://doi.org/10.1002/nme.1620240713

[14] M. Ould Ouali and M. Aberkane. Micromechanical modeling of the rolling of a A1050P aluminum sheet. International Journal of Material Forming, Vol. 2, Issue1, 2009, pp 25-36. http://dx.doi.org/10.1007/s12289-008-0387-3

[15] M. Ould Ouali. Relevance of incorporating cavity shape change in modelling the ductile failure of metals. Mathematical Problems in Engineering. Vol. (2018), Article ID 6454790, 9 pages, 2018. https://doi.org/10.1155/2018/6454790

[16] J.T. Oden, J.A.C. Martins, Models and computational methods for dynamic friction phenomena. Computer Methods in Applied Mechanics and Engineering, vol. 52, no. 1-3, 527-634, 1985. https://doi.org/10.1016/0045-7825(85)90009-X

[17] A.E. Giannakopoulos, The return mapping method for the integration of friction constitutive relations. Computers & Structures, vol. 32, no. 1, 157-167, 1989. https://doi.org/10.1016/0045-7949(89)90081-3

[18] R. Dobry, T.T. Ng, E. Petrakis, A. Seridi, General model for contact law between two rough spheres. Journal of Engineering Mechanics, vol. 117, no. 6, 1365–1381, 1991. https://doi.org/10.1061/(ASCE)0733-9399(1991)117:6(1365)

[19] Z. Mroz, A. Jarzebowski, Phenomenological model of contact slip. Acta Mechanica, vol. 102, 59-72, 1994. https://doi.org/10.1007/BF01178518

[20] R.D. Mindlin, H. Deresiewicz, Elastic spheres in contact under varying oblique forces. Journal of *Applied Mechanics, vol.* 20, no. 3, 327–344, 1953. https://doi.org/10.1115/1.4010702

[21] U. Sellgren, U. Olofsson, Application of a constitutive model for micro-slip in finite element analysis. Computer Methods in Applied Mechanics and Engineering, vol. 170, no. 1-2, 65-77, 1999. https://doi.org/10.1016/S0045-7825(98)00189-3

[22] K. Hashiguchi, Subloading surface model in unconventional plasticity. International Journal of Solids and Structures, vol. 25, no. 8, 917-945, 1989. https://doi.org/10.1016/0020-7683(89)90038-3

[23] K. Hashiguchi., S. Ozaki, Constitutive equation for friction with transition from static to kinetic friction and recovery of static friction. International Journal of Plasticity, vol. 24, 2102-2124, 2008. https://doi.org/10.1016/j.ijplas.2008.03.004

[24] J.H. Prevost, Mathematical modelling of monotonic and cyclic undrained clay behaviour. International Journal of Numerical and Analytical Methods in Geomechanics, vol. 1 , 195-216, 1977. https://doi.org/10.1002/nag.1610010206

[25] Z. Mroz, On the description of anisotropic work hardening. Journal of the Mechanics and Physics of Solids, vol. 15, no. 3, 163–175, 1967. https://doi.org/10.1016/0022-5096(67)90030-0

[26] A. Jarzębowski, Z. Mróz, Z, On slip and memory rules in elastic, friction contact problems. Acta Mechanica, vol. 102, 199–216, 1994. https://doi.org/10.1007/BF01178527

[27] Z. Mroz, S. Stupkiewicz, An anisotropic friction and wear model. International Journal of Solids and Structures, vol. 31, 1113–1131, 1994. https://doi.org/10.1016/0020-7683(94)90167-8

[28] Z. Mroz, S. Stupkiewicz, Constitutive model of adhesive and ploughing friction in metal-forming processes. International Journal of Mechanical Sciences, vol. 40, 281–303, 1998. https://doi.org/10.1016/S0020-7403(97)00055-6

[29] P. Wriggers, Computational contact mechanics. New York: John Wiley & Sons Ltd, 2006. https://doi.org/10.1007/978-3-540-32609-0

[30] X.S. Yang. Engineering Mathematics with Examples and Applications (ISBN 9780128097304), Chapter 23 - Optimization. Academic Press, 267-283, 2017. https://doi.org/10.1016/B978-0-12-809730-4.00031-8

[31] L. Anand, A constitutive model for interface friction. Computational Mechanics, vol. 12, 197–213, 1993. https://doi.org/10.1007/BF00369962

[32] K. Hashiguchi, S. Ozaki, T. Okayasu, Unconventional friction theory based on the subloading surface concept. International Journal of Solids and Structures, vol. 42, 1705–1727, 2005. https://doi.org/10.1016/j.ijsolstr.2004.08.006

[33] K. Hashiguchi, Y. Yamakawa, Introduction to finite strain theory for continuum elastoplasticity. Wiley Series in Computational Mechanics. Chichester, UK: John Wiley & Sons Ltd, 2012. https://doi.org/10.1002/9781118437711

[34] K. Hashiguchi, General description of elastoplastic deformation/sliding phenomena of solids in high accuracy and numerical efficiency: subloading surface concept. Archives of Computational Methods in Engineering, vol. 20, 361–417, 2013. https://doi.org/10.1007/s11831-013-9089-1

[35] S. Ozaki, K. Hashiguchi, Numerical analysis of stick-slip instability by a rate-dependent elastoplastic formulation for friction. Tribology International, vol. 43, 2120–2133, 2010. https://doi.org/10.1016/j.triboint.2010.06.007

[36] Z. Mroz, An attempt to describe the behavior of metals under cyclic loads using a more general workhardening model. Acta Mechanica, vol. 7, 199–212, 1969. https://doi.org/10.1007/BF01176668

[37] Z. Mroz, S. Pietruszczak, A Constitutive model for sand with anisotropic hardening rule. International Journal of Numerical and Analytical Methods in Geomechanics, vol. 7, 305-320, 1983. https://doi.org/10.1002/nag.1610070304

[38] C. Liu, G. Wang, W. Han, Effect of Slip Surface's Continuity on Slope Dynamic Stability Based on Infinite Slope Model.

Mathematics, vol. 7, no. 1, 2019. https://doi.org/10.3390/math7010058

[39] R.J. Chenari, H.K. Farahbakhsh, A. Izadi, Continuous slip surface method for stability analysis of heterogeneous vertical trenches. Scientica Iranica, vol. 27, no. 6, 2657-2668, 2020. https://doi.org/10.24200/sci.2019.21227

[40] J. Jäger, Stepwise loading of half-spaces in elliptical contact. Journal of Applied Mechanics, vol 63, 766-773, 1996. https://doi.org/10.1115/1.2823361

[41] Abaqus 2019 User's manuals. Dassault Systèmes Simulia Corp. Providence, RI, USA., 2019

[42] S.C. Tang, Z.C. Xia, F. Ren, Application of the radial return method to compute stress increments from Mroz's hardening rule. Journal of Engineering Materials and Technology, vol. 123, no. 4, 398–402, 2001. https://doi.org/10.1115/1.1395022

[43] M. Meggiolaro, J. Castro, H. Wu, On the applicability of multi-surface, two-surface and non-linear kinematic hardening models in multiaxial fatigue. Frattura Ed Integrità Strutturale, vol. 9, no. 33, 357–367, 2015. https://doi.org/10.3221/IGF-ESIS.33.39

[44] K.L. Johnson, Contact Mechanics. Cambridge University Press, Cambridge/New York, 1985.